Sensors and Materials, Vol. 36, No. 9 (2024) 3677–3690
MYU Tokyo

S & M 3758

Role of ZnO Capping Layer for Stability in Silver-nanowire-based Functional Heater Arrays

Sejin Kim,[1,2†] Dong-Geon Lee,[1,3†] Qiang Liu,[1] Mi-Jin Jin,[3] Bo Hou,[4] Seungyoung Park,[5] Ji-Yeop Kim,[1,3] Doo-Seung Um,[6,7*] and Chang-Il Kim[1**]

[1]School of Electrical and Electronics Engineering, Chung-Ang University, Seoul 06974, Republic of Korea
[2]School of Electrical Engineering, Korea Advanced Institute of Science and Technology (KAIST), Daejeon 34141, Republic of Korea
[3]Center for Multidimensional Carbon Materials (CMCM), Institute for Basic Science (IBS), Ulsan 44919, Republic of Korea
[4]School of Physics and Astronomy, Cardiff University, Cardiff CF24 3AA, Wales, United Kingdom
[5]Thin Film Materials Research Center, Korea Research Institute of Chemical Technology (KRICT), Daejeon 34114, Republic of Korea
[6]Department of Electronic Engineering, Jeju National University (JNU), Jeju 63243, Republic of Korea
[7]Faculty of Applied Energy System (Electronic Engineering), Jeju National University (JNU), Jeju 63243, Republic of Korea

(Received June 24, 2024; accepted August 14, 2024)

Keywords: silver nanowire, flexible heater, thermochromic liquid crystal, smart textile, emotional transmission

Communication technology has evolved continuously throughout human history, especially recently, for overcoming physical distancing. In addition to visual and auditory senses, the transmission of tactile sensations through the human skin holds significant potential as a novel communication method. In this paper, we propose a flexible heating device that can convey warmth at distances. A pixelated heater was developed by depositing Ag nanowires (NWs) patterned on a thin polyimide substrate. The thermal and mechanical durabilities of the Ag NWs were effectively enhanced using a ZnO film as the capping layer. In addition, we created a multifunctional heater by depositing a flexible thermochromic liquid crystal polydimethylsiloxane film on the heater, providing visual feedback on temperature changes. The resistance variations and thermal characteristics of the multifunctional heater were examined under bending to demonstrate its performance as a flexible heater. The results of this study are expected to extend the applications of this technology from simple wearable devices to multifunctional metaverse devices in various fields.

1. Introduction

Throughout human history, the evolution of communication technology has been intertwined with the progress of civilization and technological innovation. Human civilization has progressed

*Corresponding author: e-mail: dsum@jejunu.ac.kr
**Corresponding author: e-mail: cikim@cau.ac.kr
†These authors equally contribute to this paper.
https://doi.org/10.18494/SAM5137

through continuous efforts to connect with each other beyond physical distances and express and transmit profound emotions.

From the long history of handwritten letters, through the telegraph era, to the emergence of voice and video communication, and cutting-edge haptic technology, we have constantly searched for novel technologies that allow us to perceive each other's emotions in time and space.[1] For nearly a century, our primary mode of communication has centered on auditory channels, primarily relying on sound to articulate thoughts and emotions. With the advent of smartphones, video calls have become increasingly common and our interactions have become more vivid. The internet connection facilitates the use of video calls anytime and anywhere between different portable devices. In addition to voice and video communication, the latest haptic technologies attempt to create an emotional communication era through tactile transmission.[2,3] The potential impact of emotional communication interfaces transcends personal connections with profound implications for a wide array of fields, including rehabilitation medicine, assistive devices, robotics, and metaverse technology.[4–7]

The human skin is a complex sensory canvas with numerous receptors receiving a range of sensations, including temperature, pressure, and pain.[8,9] The complex interactions of these senses allow us to experience different emotions.[10–12] In particular, warmth can positively impact mental well-being and act as a key factor in enhancing emotional connections. Several essential factors must be considered when creating a device that can effectively transmit heat. In particular, high flexibility to adhere closely to the skin and rapid operation with precise temperature control are required. Moreover, the heater must be miniaturized and arrayed to enable the transmission of dynamic emotions and soft touches of affection. In this context, Ag nanowires (NWs) could be a pivotal breakthrough. Ag NWs exhibit excellent mechanical flexibility, rapid heating, high energy efficiency, and precise temperature control.[13–16]

In this study, we developed a pixelated heating device by patterning Ag NWs onto a highly flexible substrate. A thin ultraflexible polyimide (PI) substrate was used to withstand high temperatures and maximize the heat transfer efficiency to the skin.[17] A zinc oxide (ZnO) capping layer was introduced to overcome the inherent thermal durability limitations of Ag NWs, thereby greatly improving the mechanical and thermal durabilities, temperature uniformity, morphological stability to thermal stress, and heating efficiency of the heater.[18–20] In addition, we integrated thermochromic liquid crystals (TLCs) into the pixelated heating film to enable the visual expression of temperature changes, thereby allowing the use of visual effects as a multifunctional metaverse device.[21] The functional heating films that integrate thermal sensations and visual feedback can be applied to next-generation military artificial camouflage and flexible realistic display technologies.[22] The results of this study are expected to expand the application of the technology in various fields, from simple wearable devices to ultrarealistic multifunctional metaverse devices.

2. Materials and Methods

2.1 Materials

A p-type 4-in test-grade Si wafer with a thickness of approximately 525 μm was used. The PI solution was purchased from Picomax Corp., Korea. Ethanol-based solutions containing Ag NWs with lengths and diameters of 25 μm and 25 nm, respectively, were purchased from Nanopix Corp., Korea.

The polydimethylsiloxane (PDMS) shadow mask was fabricated by preparing a PDMS solution of a silicone elastomer base and a curing agent at a ratio of 10:1. The viscosity of the PDMS solution was reduced by adding 9 wt.% hexane. The solution was then placed in a vacuum chamber for 10 min to remove bubbles. Subsequently, a 40 × 40 mm^2 metal mask with 3 × 3 mm^2 square holes was prepared. The shape of the metal mask was replicated by adding the prepared PDMS solution dropwise onto the area, except for the square hole of the mask. PDMS maintained the same shape as the metal mask owing to its viscosity and surface tension and was cured on a hot plate at 70 °C for 4 h. The cured PDMS was carefully peeled from the metal mask to obtain patterned PDMS with square holes.

The solution for the thermochromic film was prepared by mixing the PDMS solution of the silicone elastomer base and the curing agent at a ratio of 10:1 and black and red TLC ink (SFXC, Newhaven, UK) at a ratio of 20:1:1. Black and red TLCs changed from black and red to white at temperatures above 27 and 47 °C, respectively. Therefore, the PDMS mixed with black and red TLCs exhibited a dark brown color at temperatures below 27 °C and changed to pink as the black TLC turned white at temperatures above 27 °C. As the temperature was further increased to more than 47 °C, even the red TLC changed to white, resulting in the color changes of the TLC layer.

2.2 Fabrications

The ultraviolet/ozone (UVO) treatment using a UV-C wavelength with an illuminance of approximately 20 mW/cm^2 was carried out at room temperature in air ambient. Ag electrodes were deposited using a thermal evaporation system (KVT-2004; KOREAVAC, South Korea). The Ag pellets (99.999% purity) were placed in a W boat. The substrate was positioned at 20 cm above the Ag pellets and rotated clockwise at 5 rpm to obtain a highly uniform film during deposition. The chamber was evacuated to a pressure below 10^{-6} Torr using rotary and cryopump. When the W boat was heated and a stable evaporation rate was achieved, the shutter in front of the substrate opened. The thickness of the Ag film was controlled by varying the deposition time.

The ZnO target (99.99%, diameter of 2 in, thickness of 1/8 in) was bonded to Cu-backed plates. Before depositing the ZnO thin film, chamber stabilization and target cleaning were performed through an Ar plasma pretreatment for 10 min. The ZnO thin films were deposited on the surface of the sample by radio frequency (RF) magnetron sputtering under the following conditions: substrate temperature of 27 °C, RF power of 60 W, operating pressure of 5 mTorr,

and Ar flow rate of 30 sccm at a substrate-to-target distance of 15 cm. The deposited ZnO thin film had a thickness of 190–210 nm.

2.3 Characterization and measurement

The surface roughness of the Ag NW pattern was examined by atomic force microscopy (NX-10, Park system). The surface and cross-sectional morphologies of the Ag NW/PI and ZnO/Ag NW/PI heater films were examined by field-emission scanning electron microscopy (FE-SEM; Sigma 300, Carl Zeiss). The electrical resistances of the Ag NW/PI and ZnO/Ag NW/PI heater devices were measured using a digital multimeter (DMM7510, Keithley). The sheet resistance was measured every 3 min with the two samples placed on a hot plate at a temperature of 250 °C and a humidity of 22%. A DC voltage was supplied to the heater device through the Ag contact at the edge of the film using a power supply. The temperature of the film was measured using an infrared thermal imager (UTi260B, UNI-T). Mechanical stability measurements were conducted using a bending test machine (ST-MO-X10-BENDING, ST1).

3. Results and Discussion

Figure 1 shows a schematic of the Ag-NW-based flexible heater array with PI as the device substrate and ZnO as the capping layer to improve thermal stability and mechanical flexibility. Here, the size of the pixel is 3 × 3 mm^2. The Si substrate was cleaned by ultrasonication in an isopropyl alcohol solution for 10 min, rinsed with deionized water, and dried under an N_2 flow.

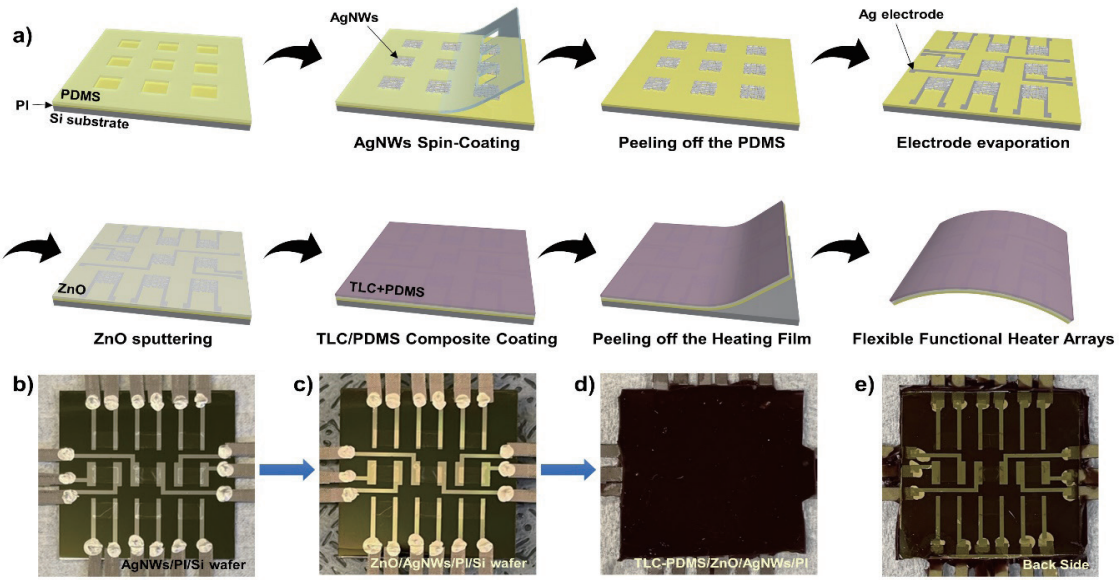

Fig. 1. (Color online) (a) Schematic of thermochromic heating pixel array film. (b–e) Optical images of actual devices during each process: (b) after attaching the Ag electrodes and Pb wires, (c) after the ZnO capping layer deposition, and (d) front and (e) back of the final device after TLC–PDMS film was stacked.

Subsequently, the Si substrate was treated with UVO for 10 min to increase the adhesion with the PI film and enhance the capillary effect for the water-assisted peeling process of the final device. The PI solution was coated using a spin coater at 2000 rpm for 30 s and cured by an annealing process at 300 °C for 30 min. The Ag NW network pattern was created on a PDMS shadow mask, patterned with a rectangular 3 × 3 array, attached to the surface of a PI film coated on a Si substrate. One drop of the ethanol-based Ag NW solution was sequentially dropped into each PDMS hole, which was used as the exposed spot of the PI film, and spin-coated at 2000 rpm for 30 s. The Ag NWs were effectively constructed and tightly attached to the substrate by annealing at 90 °C for 30 min. Ag NW networks patterned with rectangular arrays were formed after removing the PDMS shadow mask. The electrode for applying voltage to each heater cell was formed by depositing Ag through a thermal evaporator, while the metal shadow mask was aligned onto the Ag-NW-patterned substrate. Pb wires were attached to the Ag electrodes to connect each cell to an external power supply, as shown in Fig. 1(b). Additionally, a 200-nm-thick ZnO capping layer was deposited by RF sputtering to increase the thermal and mechanical stabilities of the Ag NW heating cells [Fig. 1(c)]. After the ZnO capping layer was deposited, the resistivity increased by approximately 10% from 65.8 to 72.82 Ω·cm. Additional functionality was provided to the heating film by sufficiently spreading a PDMS solution with two types of TLC on the ZnO capping layer and curing at 80 °C for 3 h. Finally, the completed device and functional heating arrays were separated from the Si substrate using a water-assisted capillary peeling-off method.[23,24] The average resistivity of each cell in the separated heater array slightly increased to 104.18 Ω·cm; this is considered to be an aftereffect of the surface curvature due to the separation from the rigid substrate. Figures 1(d) and 1(e) show the final device after separation from the Si substrate. Because the top surface was opaque to the TLC layer, the interior of the device was invisible, and the back surface clearly showed the Ag electrode deposited on the thin and semitransparent PI substrate.

Devices with and without a capping layer were fabricated and evaluated to confirm the contribution of the ZnO capping layer in improving thermal reliability. Figure 2 shows the improved thermal reliability of the device with the ZnO capping layer in the Ag-NW-based heater. The sheet resistance increased more than 323 times from 17 Ω/sq to 5.5 kΩ/sq for the sample without a capping layer after approximately 15 min and further increased to more than 105 times after 18 min, reaching a point where it could no longer be measured, as shown in Fig. 2(a). Figure 2(b) shows an SEM image of the Ag NW network film after annealing at 250 °C for 18 min on a hot plate. Several Ag NW connections were broken. When a ZnO layer was stacked on the Ag NW networks, the sheet resistance increased by approximately 1.2 times from 60 to 76 Ω/sq after 15 min and increased only four times after 30 min on a hot plate at 250 °C and a humidity of 22%. This clearly shows the positive effect of the ZnO capping layer on the high-temperature reliability, which can be ascribed to the high thermal conductivity of the ZnO thin film that appropriately disperses heat.[25]

The thermal response of the device and the role of the ZnO capping layer after the peeling process were analyzed from the temperatures of the Ag NW/PI and ZnO/Ag NW/PI flexible pixel heaters under an applied voltage. The resistivity of the pixels of the two devices measured by the two-wire method was ~69 Ω·cm. An input voltage of 1–3 V was applied for 60 s at

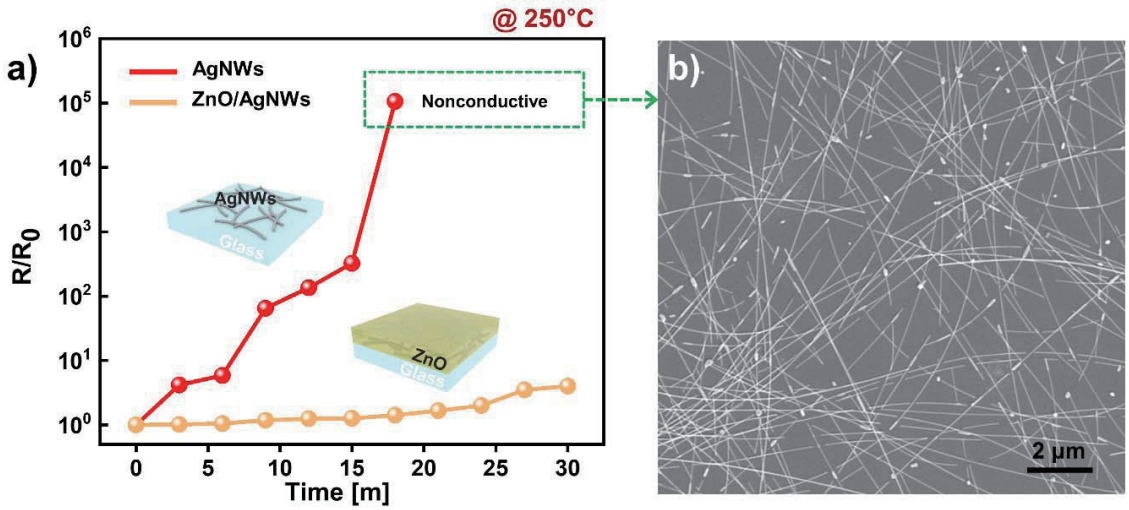

Fig. 2. (Color online) (a) High-temperature reliability with and without a ZnO capping layer in the Ag NW network. Continuous sheet resistance changes were observed with the sample on a hot plate at 250 °C. (b) SEM image of the Ag NW heater without a ZnO capping layer after 15 min of heating on a hot plate of 250 °C. The Ag NWs are partially broken or melted.

intervals of 0.5 V. Figures 3(a) and 3(b) present the temperature profiles of the Ag NW/PI- and ZnO/Ag NW/PI-structured devices, respectively. The inset in Fig. 3(b) shows a thermal image of the heater with a ZnO capping layer at an applied voltage of 1.5 V. At the input voltage of 1 V, the heater without ZnO reached a temperature of 39.8 °C after 60 s, whereas that with ZnO reached 43.1 °C. When the input voltage was increased by 2 V, the temperature of the ZnO/Ag NW/PI-structured device reached 87.7 °C, which is also 10% higher than the heating of the Ag NW/PI-structured device. The results can be explained using the heat transfer equation for Joule heating based on heaters composed of Ag NWs, as follows:[26]

$$I^2R = \left(m_1C_1 + m_2C_2\right)\frac{dT(t)}{dt} + A\left(h_1 + h_2\right)\Delta T(t) + \sigma A\left(\varepsilon_1 + \varepsilon_2\right)\left(T(t)^4 - T_0^4\right) + \alpha_{cond}\Delta T(t), \quad (1)$$

where indexes 1 and 2 correspond to the network and substrate, respectively. The basic concept in Eq. (1) is energy conservation. The term on the left represents the power input from the heater, I is the current, and R is the system resistance. The first term on the right is the heat per unit time to the network and substrate, which increases the temperature of the sample. C is the specific heat, and m is the mass. The second term represents the heat loss per unit time due to convection, where h is the convective heat-transfer coefficient, and A represents the area of the network. The areas of the network and substrate between the electrodes are assumed to be equal. $\Delta T(t)$ is the difference between the instantaneous sample temperature and ambient temperature. The third term refers to the heat loss per unit time due to radiation, and σ and ε represent the Stefan–Boltzmann constant and emissivity, respectively. The last term is the heat loss per unit time, which is mainly ascribed to the conduction through the wires. α_{cond} denotes the heat-transfer

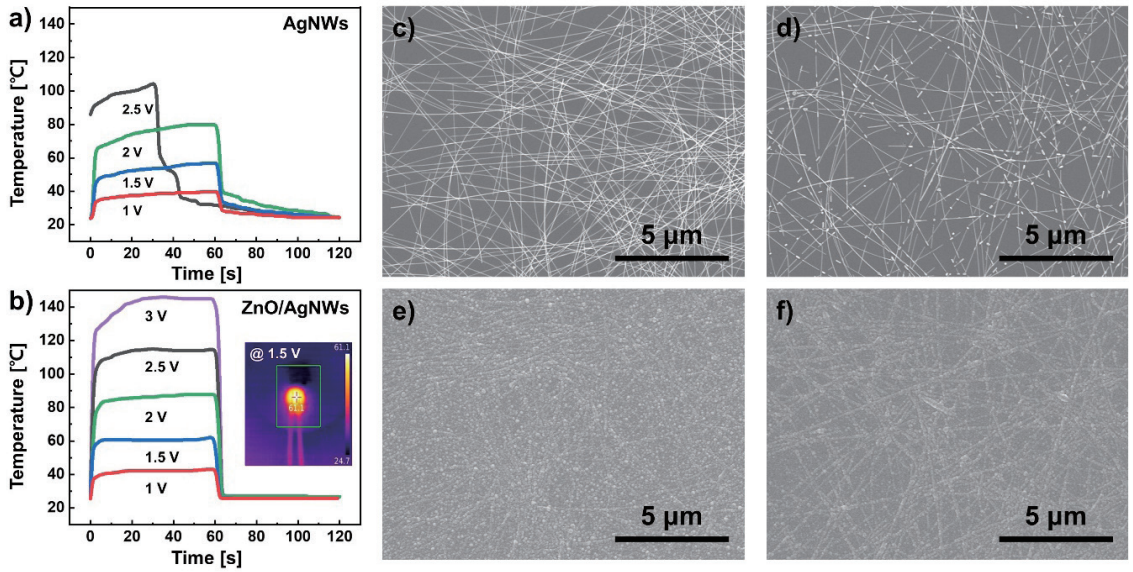

Fig. 3. (Color online) (a and b) Temperature change in the Ag NW network cell with/without ZnO capping layer for various applied voltages. The inset of (b) shows the thermal image of the cell at the applied voltage of 1.5 V. (c and d) SEM images of the Ag NW network cells without the ZnO capping layer (c) before and (d) after the voltage of 2.5 V was applied. (e and f) SEM images of Ag NW network cells with ZnO capping layer (e) before and (f) after the voltage of 2.5 V was applied.

constant by conduction. By simplifying Eq. (1), we obtain

$$T(t) \approx T_0 + \frac{V^2}{\alpha RA}\left[1 - \exp\left(-\frac{\alpha}{\frac{m_2 C_2}{A}}t\right)\right], \tag{2}$$

where α denotes the heat-transfer constant considering the heat loss parameter.[27]

$$\alpha = (h_1 + h_2) + 4(\varepsilon_1 + \varepsilon_2)\sigma T_0^3 + \alpha_{cond} \tag{3}$$

Here, as a steady state is achieved at a high T, the exponential term can be ignored; therefore, the steady-state temperature consists only of the initial temperature (room temperature), applied voltage, heat-transfer constant, resistance, and area. Therefore, if the initial temperature, voltage, resistance, and area are fixed, a higher steady-state temperature can be reached by reducing α. In addition, α has a positive correlation with the convection coefficient; thus, it can be reduced by preventing convection. The ZnO capping layer limits convection. The heat generated from the ZnO/Ag NW/PI structure blocks direct contact with air and prevents convection, whereas that from the Ag NW/PI structure through Joule heating is directly in contact with air and prompts active convection. Therefore, α is lower in the heater with a capping layer, facilitating higher steady-state temperatures. At an applied voltage of 2.5 V, the temperature decreases in the Ag

NW/PI heater started at 40 s, even though the input voltage was applied for 60 s. This indicates that the device did not generate heat and was broken. Figures 3(c) and 3(d) show the SEM images of the surface of the Ag NW/PI heater before and after applying a voltage of 2.5 V. The NW networks were well formed before applying the voltage but were partially melted and disconnected by the high temperature at the junction after applying the voltage. Consequently, the electrical resistivity increases by approximately 21 times to 1.5 kΩ·cm after the voltage was applied. Meanwhile, the ZnO/Ag NW/PI heater maintained its good operation at voltages exceeding 2.5 V. Figures 3(e) and 3(f) show the SEM images of the surface of the ZnO/Ag NW/PI heater before and after applying a voltage of 2.5 V for 60 s. A Ag NW network silhouette was observed on the ZnO layer, which was maintained even after an input voltage of 3 V (60 s) was applied. Moreover, the electrical resistivity was maintained at ~69 Ω·cm. In summary, the ZnO capping layer reduced convection phenomena, resulting in a high steady-state temperature, and enhanced the thermal stability of AgNW networks.

Figure 4(a) shows the results of repeated tests with 60 s of heating and 60 s of cooling under an applied voltage of 2 V for the samples with and without the ZnO capping layer. The devices reached the desired temperature without significant performance degradation. The maximum temperature for both devices slightly increased after 10 cycles because of the slight decrease in the resistance of the heater as the network junctions moved closer together by Joule heating. In addition, the response time, defined as the time taken to reach a steady-state temperature from room temperature, is also an important factor for evaluating the heating performance of devices. The temperature increase and decrease times at the device without a capping layer were approximately 15 s, respectively, whereas those with a capping layer were approximately 5 s, such those shown in Figs. 4(b) and 4(c). This is considered to be due to the difference in specific heat capacity between the ZnO and air in contact with the AgNW networks as the heating part of the device. It is generally known that the specific heat capacity of air is roughly twice as high as that of ZnO. Therefore, the temperature change occurs faster in the device with a ZnO capping layer.

Ag NWs and TLC–PDMS composite film were sequentially coated on a 2.5 × 2.5 cm^2 glass substrate, as shown in Fig. 5, to confirm the properties of the TLC–PDMS composite film.

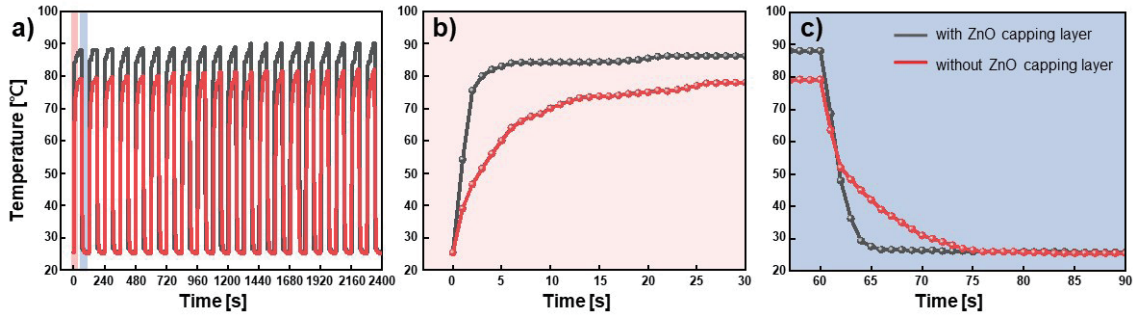

Fig. 4. (Color online) (a) Heating curve of the Ag NW network cells with and without the ZnO capping layer with the cyclic on–off voltage of 2 V. (b) Temperature increase with voltage application. (c) Temperature decrease as the voltage was turned off. The red line is without the ZnO capping layer and the gray line is with the ZnO capping layer.

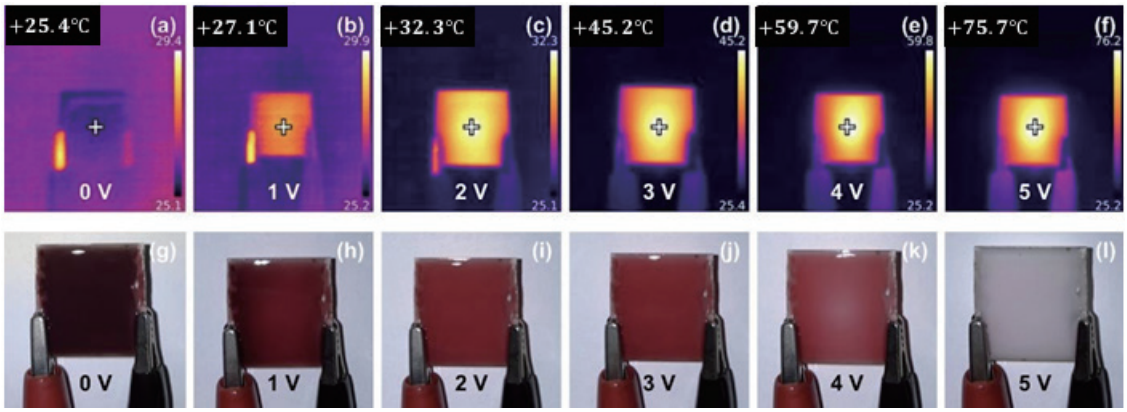

Fig. 5. (Color online) Color change of the thermochromic film on the glass substrate in accordance with the voltage application.

Figure 5 shows the color change of the TLC–PDMS composite film in accordance with the temperature. Voltage was applied to both sides of the sample from 0 to 5 V for 3 min to check the color change over time. The surface temperature of the sample before applying the initial voltage was room temperature, and the surface was dark brown. The temperature of the substrate increased with an increase in applied voltage, reaching 75.7 °C at an applied voltage of 5 V, resulting in a color change of the sample surface from red to pink, and finally to white. This suggests that a wider variety of multifunctional and discoloration heaters could be produced by stacking new functional composite films.

In addition to improving the thermal properties, the ZnO capping layer provided high mechanical stability for flexible heater devices.[26] Figure 6 shows the results of the evaluation of the mechanical stability of the multifunctional heating device through external and internal bending tests. The change in resistance of the cells is expressed as $\Delta R = (R - R_0)/R_0$, where R_0 is the initial resistance and R is the resistance measured after the bending test. The device used for the evaluation was a heater deposited onto the final TLC–PDMS composite layer, and the effect of the capping layer on the mechanical reliability of the final device was investigated. The change in the resistance was measured using the two-wire method. Figure 6(a) shows the change in resistance with decreasing outer bending radius, that is, with increasing stress applied to the cell. Minimal changes in the resistance were noted when the outer radius was greater than 1.3 cm. As the outer radius was decreased to less than 1.3 cm, the resistance of the heater gradually increased. Compared with the initial resistance, the resistance increased rapidly with an outer radius of 0.5 cm for the heater without a capping layer and increased by approximately 6% with an outer radius of 0.1 cm. In contrast, there were no significant resistance changes in terms of the overall outer bending radius for the sample with the capping layer. In particular, the resistance only increased by approximately 2% at an outer bending radius of 0.1 cm. Figure 6(b) shows the change in resistance with respect to the internal bending radius. A slight change in resistance was observed at an internal radius of 1.3 cm. The resistance gradually increased as the inner radius was decreased to up to 0.6 cm and increased rapidly as the inner radius was decreased to below 0.4 cm, resulting in a resistance increase of approximately 10% at an inner radius of 0.1

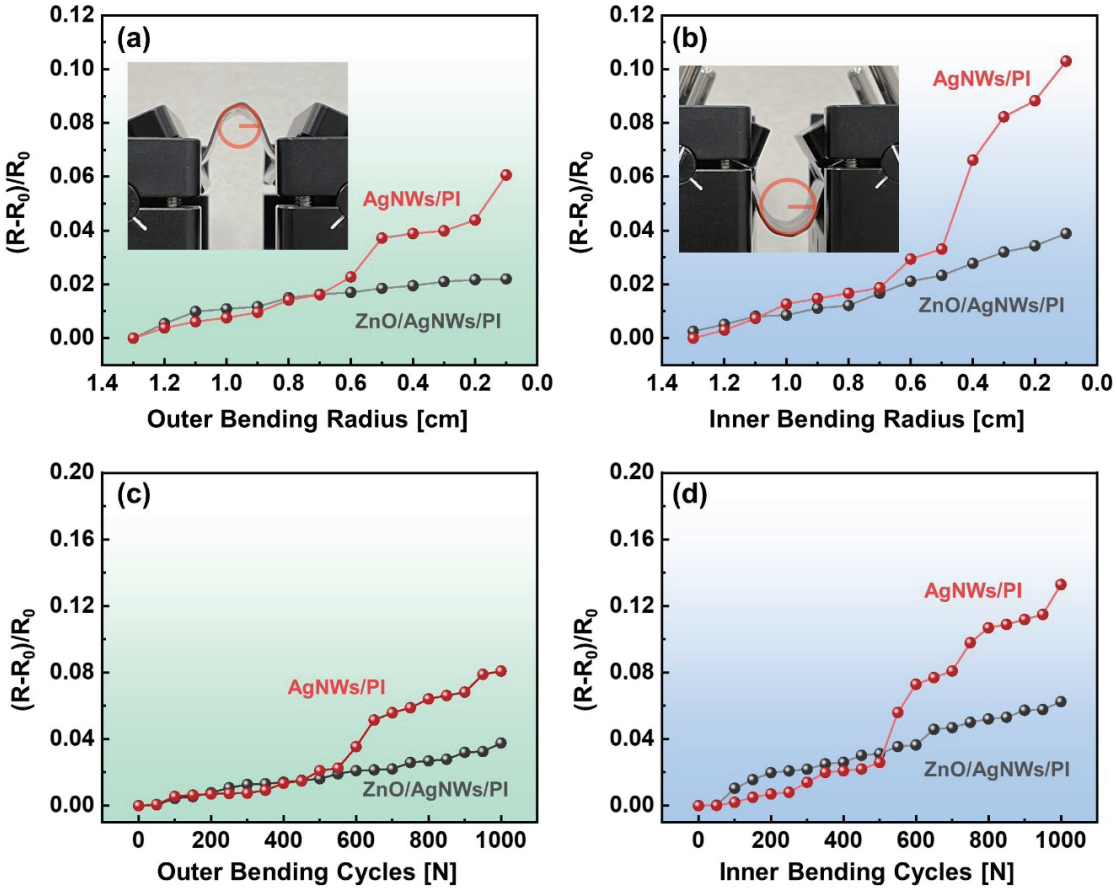

Fig. 6. (Color online) Mechanical stability of the flexible thermochromic heating pixel arrays with and without the ZnO capping layer. (a and b) Resistance changes in terms of the (a) outer and (b) inner bending radii. (c and d) Resistance changes with the number of (c) outer and (d) inner bending cycles with the bending radius of 0.5 cm.

cm. In contrast, a constant resistance change was observed without rapid change for the sample with the capping layer. The final resistance change was only approximately 4%, similar to that in the outer radius experiment. The experimental result shows that the capping layer provides high mechanical and thermal stability to the flexible heating device. The difference in the resistance change in the outer and internal bending experiments is ascribed to the structural difference in the device, whereby the Ag NW networks were coated on a thin PI substrate and a thick discoloring film was laminated on the top. Consequently, higher stress was applied to the Ag NW network by internal bending. Figures 6(c) and 6(d) show the change in resistance depending on the number of outer and internal bending cycles of up to 1000 times. In the external and internal bending cycle tests, the resistance of Ag NW/PI increased rapidly at approximately 600 cycles, whereas that of ZnO/Ag NW/PI did not show a significant increase. After 1000 outer radius bending tests, the resistance increased by 8% without the capping layer and 4% with the capping layer. The internal radius bending test showed an increase in resistance of approximately 13% without a capping layer and only 6% with a capping layer after 1000 bending cycles. These

results clearly show that the capping layers facilitate the flexible heaters to maintain their electrical properties in response to mechanical deformations.

Figure 7 shows a multifunctional film composed of 3 × 3 heating cells that can depict colors. Figure 7(a) shows a multifunctional film with a dark brown surface without applied voltage. Figure 7(b) shows a schematic of the composition of each layer of the multifunctional film. Figures 7(c) and 7(e) show that heat was generated in the cells with applied voltages of 1 and 2 V, respectively, even when the film was bent, resulting in the color change of the TLC–PDMS composite layer. When the voltage was applied to five out of the nine cells, forming a cross shape, all the cells generated heat well, as shown in Figs. 7(d) and 7(f). The color of each cell changed from dark brown to bright red and white with the applied voltages of 1 and 2 V, respectively. The cells applied with 2 V exhibited two colors with white in the center and red on the outside. Although the temperature increased only in the cells patterned with Ag NWs, the results denote that the temperature is transmitted to the surrounding area owing to the high thermal conductivity of the ZnO capping layer. The color change and heat uniformity of the cell with the multifunctional film with and without the ZnO capping layer are shown in Fig. 8. As the PI substrate is a material with a low thermal conductivity, sharp color changes are noted for the sample without the ZnO capping layer, as shown in Fig. 8.

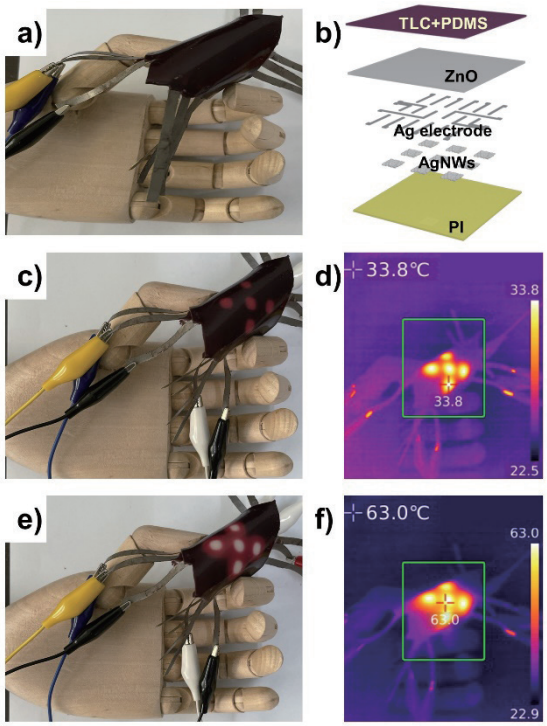

Fig. 7. (Color online) Ag-NW-based heating pixel array film with a thermochromic function. (a) Image of the film without an applied voltage. (b) Schematic of the film structure. (c and d) Color change and temperature change of the film under the applied voltage of 1 V. (e and f) Color change and temperature change of the film under the applied voltage of 2 V.

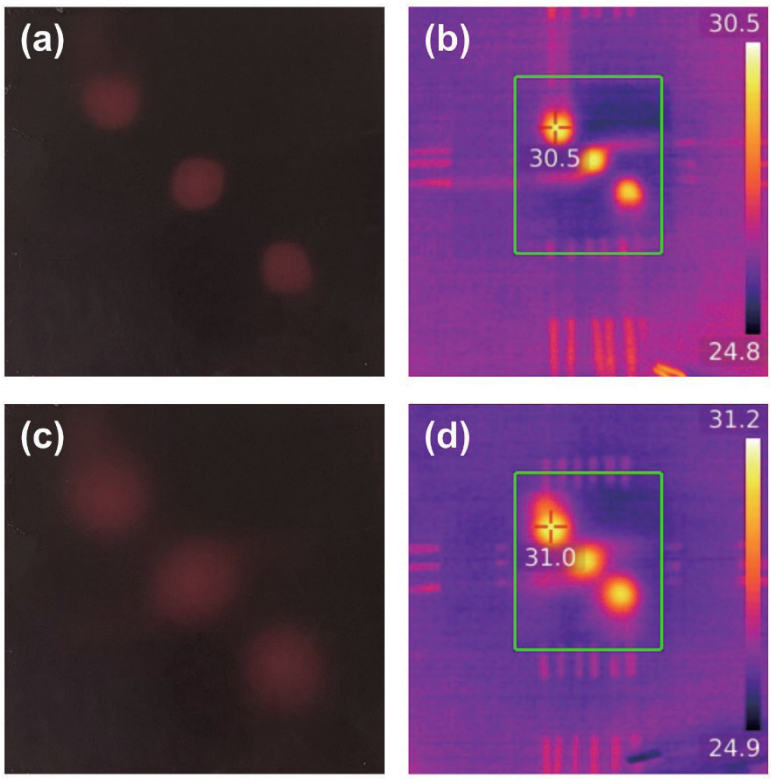

Fig. 8. (Color online) Optical and thermal images of a multifunctional film's thermal response. (a and b) Film without the ZnO capping layer; (c and d) film with the capping layer. The optical images (a and c) reveal the color changes upon heating, and the corresponding thermal images (b and d) display the temperature distribution across the cells.

4. Conclusions

We successfully fabricated a flexible and multifunctional heater array to transmit emotions through colors by integrating a heating array and TLC–PDMS composite film. A multiheating cell array was produced by patterning Ag NWs using a PDMS shadow mask through a facile spin-coating method. The thermal and mechanical durabilities were enhanced by introducing a ZnO capping layer between the Ag NW heating array and TLC–PDMS composite films. Rigorous evaluations confirmed the pivotal role of the ZnO capping layer in ensuring the longevity and stability of the device under various thermal and mechanical stressors. Moreover, the functional composite film responded to different temperatures while maintaining elasticity by mixing two types of TLC to detect different temperatures and PDMS with flexible and stretchable characteristics. To ensure that the film remains attached securely to gloves and the hands, flexibility of the film was achieved through integration on the PI substrate. Overall, the results of this study demonstrated the applicability of the proposed film in emotion transmission because it can deliver various types of localized heat to a person's skin, which can be maximized through heat switching and visualization functions of the film. This research contributes to the development of flexible electronic devices with improved thermal and mechanical stabilities and shows potential for application in various fields, such as wearable technology, flexible displays, and smart textiles.

Acknowledgments

This research was supported by the Chung-Ang University Research Grants in 2021, the Institute for Basic Science (IBS-R019-Y1) and "Regional Innovation Strategy (RIS)" through the National Research Foundation of Korea (NRF) funded by the Ministry of Education (MOE) (2023-RIS009).

Author contributions

Sejin Kim: Conceptualization, Methodology, Formal Analysis, Investigation, Data Curation, Visualization, Writing - original draft; Dong-Geon Lee: Methodology, Investigation, Data Curation, Visualization, Writing - original draft; Qiang Liu: Conceptualization, Formal Analysis, Methodology; mi-Jin Jin: Methodology, Investigation, Resources; Bo Hou: Conceptualization, Methodology, Writing - review and editing; Seungyoung Park: Methodology, Visualization, Writing - review and editing; Ji-Yeop Kim: Methodology, Visualization; Doo-Seung Um: Conceptualization, Methodology, Validation, Resources, Visualization, Writing - review and editing, Supervision, Funding acquisition; Chang-Il Kim: Conceptualization, Writing - review and editing, Supervision, Project administration, Funding acquisition.

Conflicts of interest

The authors declare no conflicts of interest.

References

1 T.-H. Yang, J. R. Kim, H. B. Jin, H. J. Gil, J.-H. Koo, and H. J. Kim: Adv. Funct. Mater. **31** (2021) 2008831. https://doi.org/10.1002/adfm.202008831
2 X. Yu, Z. Xie, Y. Yu, J. Lee, A. Vazquez-Guardado, H. Luan, J. Ruban, X. Ning, A. Akhtar, D. Li, B. Ji, Y. Liu, R. Sun, J. Cao, Q. Huo, Y. Zhong, C. Lee, S. Kim, P. Gutruf, C. Zhang, Y. Xue, Q. Guo, A. Chempakasseril, P. Tian, W. Lu, J. Jeong, Y. Yu, J. Cornman, C. Tan, B. Kim, K. Lee, X. Feng, Y. Huang, and J. A. Rogers: Nature **575** (2019) 473. https://doi.org/10.1038/s41586-019-1687-0
3 K. Parida, H. Bark, and P. S. Lee: Adv. Funct. Mater. **31** (2021) 2007952. https://doi.org/10.1002/adfm.202007952
4 Y. Al-Handarish, O. M. Omisore, T. Igbe, S. Han, H. Li, W. Du, J. Zhang, and L. Wang: Adv. Mater. Sci. Eng. **2020** (2020) 4047937. https://doi.org/10.1155/2020/4047937
5 S. Choi, J. Park, W. Hyun, J. Kim, J. Kim, Y. B. Lee, C. Song, H. J. Hwang, J. H. Kim, T. Hyeon, and D.-H. Kim: ACS Nano **9** (2015) 6626. https://doi.org/10.1021/acsnano.5b02790
6 R. Yunus, S. Ali, Y. Ayaz, M. Khan, S. Kanwal, U. Akhlaque, and R. Nawaz: IEEE Access **8** (2020) 35172. https://doi.org/10.1109/ACCESS.2020.2975149
7 A. Adilkhanov, M. Rubagotti, and Z. Kappassov: IEEE Access **10** (2022) 91923. https://doi.org/10.1109/ACCESS.2022.3202986
8 M. Ha, S. Lim, J. Park, D.-S. Um, Y. Lee, and H. Ko: Adv. Funct. Mater. **25** (2015) 2841. https://doi.org/10.1002/adfm.201500453
9 O. Ozioko, R. Dahiya: Adv. Intell. Syst. **4** (2022) 2100091. https://doi.org/10.1002/aisy.202100091
10 F. Zhang, Y. Zang, D. Huang, C. Di, and D. Zhu: Nat. Commun. **6** (2015) 8356. https://doi.org/10.1038/ncomms9356
11 Z. Sun, M. Zhu, X. Shan, and C. Lee: Nat. Commun. **13** (2022) 5224. https://doi.org/10.1038/s41467-022-32745-8

12 Y. Huang, J. Zhou, P. Ke, X. Guo, C. K. Yiu, K. Yao, S. Cai, D. Li, Y. Zhou, J. Li, T. H. Wong, Y. Liu, L. Li, Y. Gao, X. Huang, H. Li, J. Li, B. Zhang, Z. Chen, H. Zheng, X. Yang, H. Gao, Z. Zhao, X. Guo, E. Song, H. Wu, Z. Wang, Z. Xie, K. Zhu, and X. Yu: Nat. Electron. **6** (2023) 1020. https://doi.org/10.1038/s41928-023-01115-7

13 S. Kang, S. Cho, R. Shanker, H. Lee, J. Park, D. S. Um, Y. Lee, and H. Ko: Sci. Adv. **4** (2018) eaas8772. https://doi.org/10.1126/sciadv.aas8772

14 S. Mun, S. Yun, S. Nam, S. K. Park, S. Park, K. B. J. Park, J. M. Lim, and K.-U. Kyung: IEEE Trans. Haptic **11** (2018) 15. https://doi.org/10.1109/TOH.2018.2805901

15 S. Hong, H. Lee, J. Lee, J. Kwon, S. Han, Y. D. Suh, H. Cho, J. Shin, J. Yeo, and S. H. Ko: Adv. Mater. **27** (2015) 4744. https://doi.org/10.1002/adma.201500917

16 P.-H. Wang, S.-P. Chen, C.-H. Su, and Y.-C. Liao: RSC Adv. **5** (2015) 98412. https://doi.org/10.1039/C5RA19804F

17 C. Yi, W. Li, S. Shi, K. He, P. Ma, M. Chen, and C. Yang: Sol. Energy **195** (2020) 340. https://doi.org/10.1016/j.solener.2019.11.048

18 B. Sun, R. Xu, X. Han, J. Xu, W. Hong, Y. Xu, Z. Fu, H. Zhu, X. Sun, J. Wang, P. Cui, J. Chang, J. Xiong, and K. Qian: npj Flex. Electron. **6** (2022) 48. https://doi.org/10.1038/s41528-022-00182-8

19 M. Wang, M. Zhang, L. Pang, C. Yang, Y. Zhang, J. Hu, and G. Wu: J. Colloid Interface Sci. **537** (2019) 91. https://doi.org/10.1016/j.jcis.2018.10.105

20 L. Bardet, D. T. Papanastasiou, C. Crivello, M. Akbari, J. Resende, A. Sekkat, C. Sanchez-Velasquez, L. Rapenne, C. Jiménez, D. Muñoz-Rojas, A. Denneulin, and D. Bellet: Nanomaterials **11** (2021) 2785. https://doi.org/10.3390/nano11112785

21 K. Li, Z. Li, Z. Xiong, Y. Wang, H. Yang, W. Xu, L. Jing, M. Ding, J. Zhu, J. S. Ho, and P.-Y. Chen: Adv. Funct. Mater. **32** (2022) 2110534. https://doi.org/10.1002/adfm.202110534

22 J. Lee, H. Sul, Y. Jung, H. Kim, S. Han, J. Choi, J. Shin, D. Kim, J. Jung, S. Hong, and S. H. Ko: Adv. Funct. Mater. **30** (2020) 2003328. https://doi.org/10.1002/adfm.202003328

23 P. Li, X. Huang, Y.-P. Zhao: Nat. Commun. **14** (2023) 6150. https://doi.org/10.1038/s41467-023-41922-2

24 D.-S. Um, Y. Lee, T. Kim, S. Lim, H. Lee, M. Ha, Z. Khan, S. Kang, M. P. Kim, J. Y. Kim, and H. Ko: ACS Appl. Mater. Interfaces **12** (2020) 32154. https://doi.org/10.1021/acsami.0c06851

25 R. Yan, T. Takahashi, H. Zeng, T. Hosomi, M. Kanai, G. Zhang, K. Nagashima, and T. Yanagida: ACS Appl. Electron. Mater. **3** (2021) 2925. https://doi.org/10.1021/acsaelm.1c00428

26 M. Lagrange, T. Sannicolo, D. Muñoz-Rojas, B. Guillo Lohan, A. Khan, M. Anikin, C. Jiménez, F. Bruckert, Y. Bréchet, and D. Bellet: Nanotechnology **28** (2016) 055709. https://doi.org/10.1088/1361-6528/28/5/055709

27 A. Khan, V. H. Nguyen, D. Muñoz-Rojas, S. Aghazadehchors, C. Jiménez, N. D. Nguyen, and D. Bellet: ACS Appl. Mater. Interfaces **10** (2018) 19208. https://doi.org/10.1021/acsami.8b03079